Comprehensive characterisation and analysis of PV module performance under real operating conditions

Louwen, Atse; de Waal, Arjen C.; Schropp, Ruud E.I.; Faaij, André P.C.; van Sark, Wilfried G.J.H.M.

Published in:
Progress in Photovoltaics: Research and Applications

DOI:
10.1002/pip.2848
10.1002/pip.2848

Document Version
Publisher's PDF, also known as Version of record

Publication date:
2017

Progress in PHOTOVOLTAICS

PROGRESS IN PHOTOVOLTAICS: RESEARCH AND APPLICATIONS
Prog. Photovolt: Res. Appl. 2017; **25:**218–232
Published online 8 December 2016 in Wiley Online Library (wileyonlinelibrary.com). DOI: 10.1002/pip.2848

RESEARCH ARTICLE

Comprehensive characterisation and analysis of PV module performance under real operating conditions

Atse Louwen[1] *, Arjen C. de Waal[1], Ruud E. I. Schropp[2], André P. C. Faaij[3] and Wilfried G. J. H. M. van Sark[1]

[1] Copernicus Institute of Sustainable Development, Utrecht University, Heidelberglaan 2, 3584CS Utrecht, The Netherlands
[2] Department of Applied Physics, Eindhoven University of Technology (TU/e), P.O. Box 513, 5600MB Eindhoven, The Netherlands
[3] Energy & Sustainability Research Institute, University of Groningen, Blauwborgje 6, P.O.Box 9700 AE Groningen, The Netherlands

ABSTRACT

The specifications of photovoltaic modules show performance under standard testing conditions (STC), but only limited information relating to performance at non-STC conditions. While performance is affected by irradiance, temperature, spectral composition of irradiance, angle-of-incidence of the irradiance and other parameters, specifications only partly give detail to consumers or retailers about the effect of irradiance and temperature.

In this study, we characterise and analyse the performance of eight different, commercially available photovoltaic modules. We establish the effect of four different parameters on module performance: irradiance, temperature, spectral composition of irradiance (via the parameter average photon energy) and angle-of-incidence, by performing linear and nonlinear optimisation of physical or empirical models. Furthermore, we characterise the operating conditions and analyse the seasonal and annual development and contribution of the four parameters to energy losses or gains relative to STC operating conditions. We show a comprehensive way of presenting the deviation of performance from STC, combining the variation in operating conditions and the resulting variation in performance.

Our results show that some effects on performance are attributable to the semiconductor material used in the modules (spectral composition and temperature), while especially angle-of-incidence effects seem more related to the type of glass used on as the front cover of the module. Variation in irradiance and module temperature generally affect performance the strongest, resulting in a performance effect ranging from +2.8% to –3.2% and –0.5% to –2.2%, respectively. The combined effect of all parameters results in an annual yield deviation ranging from +1.2% to –5.9%. © 2016 The Authors. *Progress in Photovoltaics: Research and Applications* published by John Wiley & Sons Ltd.

KEYWORDS

photovoltaics; performance; outdoor; temperature; spectral effects; irradiance; angle-of-incidence

***Correspondence**

Atse Louwen, Copernicus Institute of Sustainable Development, Utrecht University, Heidelberglaan 2, 3584CS Utrecht, The Netherlands.

E-mail: a.louwen@uu.nl

Received 26 April 2016; Revised 27 September 2016; Accepted 31 October 2016

1. INTRODUCTION

The current market for photovoltaic (PV) modules is quite homogeneous, with 90% of the market consisting of conventional, diffused junction monocrystalline and polycrystalline silicon modules [1]. More advanced types of PV modules are only gradually entering the market but are expected to gain larger market shares in the medium to long term future. One of those alternative module types is the silicon heterojunction module, currently produced mainly by Panasonic (since their acquisition of Sanyo) as the Heterojunction with Intrinsic Thin-layer (HIT; [2]) module. Other alternative PV modules include those based on thin-film amorphous silicon (a-Si), cadmium telluride (CdTe), copper indium gallium selenide (CIGS) and copper indium selenide (CIS) and on the longer term, perovskites. This variety of available module types means that selecting the right module type for the right location becomes more complex, as the optimal balance between module cost and energy yield determine the best business case, among other parameters.

The specifications of PV modules commonly show performance under standard testing conditions (STC), which are the following: irradiance of 1000 W/m^2, spectral composition of light conforming to an airmass of 1.5 and a module temperature of 25°C [3]. Testing at these condi-

tions results in a measurement of the rated power output or watt-peak power of the PV module. Additionally, specification sheets report some performance parameters at non-STC conditions: the nominal operating cell temperature (NOCT), the temperature coefficient of power, current and voltage, and sometimes the performance of the module as a function of light intensity as well. Although these specifications thus accurately describe the performance of the module under STC conditions and give some information on the effect of variations in some parameters, they do not offer much insight in the energy yield of the modules under realistic, outdoor conditions. Furthermore, the effect of other parameters on module performance, like spectral variation, angle-of-incidence (AOI) and effect of increased relative amounts of diffuse irradiance, is not described by these specifications.

In this study, we compare the performance of eight different PV module technologies and aim to establish the effect of four different parameters on PV module performance for all eight PV modules, namely irradiance intensity, module temperature, average photon energy (APE; [4]), AOI and the ratio of direct to total irradiance. Furthermore, we characterise the operating conditions under which the PV modules operate for our test-facility in Utrecht, the Netherlands, to show the effect of deviation from STC conditions on the performance of the PV modules, and the annual energy yield compared with a reference yield that can be calculated based on the rated watt-peak power output and annual insolation. We analyse the performance as a function of each parameter by filtering data around STC conditions and varying only the parameter investigated. The data was obtained over a period of approximately 1.5 years of continuous measurements between 2014 July and 2016 January.

With this study, we aim to characterise the operating conditions at a North-Western European location and compare the performance of a variety of PV module technologies under these conditions. We propose a general method that can be used to characterise PV modules under realistic operating conditions, not restricted to location. The resulting method should allow for a more accurate determination of which type of PV module is most suited for the respective installation location.

2. METHODS

2.1. Test system and data acquisition

The measurements for this study were performed at the campus of Utrecht University, Utrecht, the Netherlands, with the Utrecht Photovoltaic Outdoor Test facility (UPOT) described in [5]. The test facility is located at the top of an eight-storey building, at a height of about 36 m, at a longitude of 5.2°E and latitude of 52.1°N. The facility operates year round, 24 h per day, performing measurements on a set of PV modules, with a variety of irradiance and atmospheric sensors. Measurements of PV module performance is performed at in-plane irradiance values above 50 W/m^2.

2.1.1. PV modules

The test facility is equipped with 23 different modules, of a variety of PV technologies. Commercial modules of technologies like mono-crystalline and poly-crystalline PV modules are installed, including one pair of the same *n*-type mono-crystalline silicon modules. Thin film technologies are represented in the form of amorphous silicon (a-Si/a-Si tandem), CdTe and copper indium (gallium) selenide (CI(G)S). Also, a pair of the same silicon heterojunction (SHJ) modules is installed. Table I gives a description of the main STC parameters of all the modules observed. All modules are installed on a frame of roughly 12 by 3.6 m that is tilted by 37° with respect to the horizontal plane. From the PV modules, we measure current-voltage (IV) curves at time intervals of 2 min, with an Eko Instruments MP160 IV Curve tracer [6]. In between IV curve measurements, the modules are kept at maximum power point (MPP) by module-level power optimizers. Combined with the measurement of the IV curve, back-of-module (BOM) temperature is obtained by measurement with a thermo-couple sensor fixed to the back of each PV module, and an irradiance measurement is taken from an Eko Instruments pyranometer installed in the plane of the PV modules.

Table I. Overview of the modules installed at the Utrecht Photovoltaic Outdoor Test facility. Data taken from the module specification sheets.

Parameter	H1	M1	P1	P2	A1	CT1	CG1	CS1
Type	SHJ	Mono	Poly	Poly	a-Si/a-Si tandem	CdTe	CIGS	CIS
Area (m^2)	1.39	1.63	1.58	1.64	1.45	0.72	1.07	1.09
Rated power P_{mpp} (W)	245	265	225	240	100	77.5	110	120
Current at rated power I_{mpp} (A)	7.14	8.55	7.69	8.03	5.71	1.61	5.61	2.79
Voltage at rated power V_{mpp} (V)	34.4	31.0	29.7	29.9	17.5	48.3	19.6	43.1
Short-circuit current I_{sc} (A)	7.73	8.93	8.25	8.47	6.79	1.84	6.70	3.18
Open-circuit voltage V_{oc} (V)	42.7	39.0	37.1	37.0	23.8	60.7	25.1	59.7
I_{sc} temperature coefficient α (%/K)	0.03	0.04	0.04	0.05	0.08	0.04	0.00	0.00
V_{oc} temperature coefficient β (%/K)	–0.25	–0.33	–0.36	–0.32	–0.33	–0.24	–0.36	–0.37
P_{mpp} temperature coefficient γ (%/K)	–0.30	–0.42	–0.43	–0.41	–0.20	–0.25	–0.45	–0.39

CdTe, cadmium telluride; CIGS, copper indium gallium selenide; CIS, copper indium selenide.

DOI: 10.1002/pip

Table II. Overview of ranges used to filter data for investigation of the effect of different parameters on PV module performance.

Parameter investigated	Irradiance (W/m^2)	Temperature (°C)	APE[a] (eV)	AOI (°)	Clear-sky index
Irradiance (W/m^2)		20.5–29.5	1.848–1.904	0–57	
Temperature (°C)	950–1050		1.848–1.904	0–57	0.9–1.1
APE (eV)	950–1050	7.5–42.5		0–57	Manual[b]
AOI (°)	950–1050	20.5–29.5	1.848–1.904		Manual[b]

[a] APE was determined from spectra that were measured in the wavelength range from 350 to 1050 nm.

[b] For analysis of effect of APE and AOI, we manually selected measurements from clear sky days. See section 2.3 for a discussion.

APE, average photon energy; PV, photovoltaic; AOI, angle-of-incidence.

2.1.2. Sensors

Aside from the module measurements, UPOT gathers data with a variety of sensors. In-plane we measure irradiance with three pyranometers, the measurements of which are used for cross-validation. Also, solar spectral irradiance is measured with a spectroradiometer that measures spectral irradiance in the wavelength range of 350–1050 nm. On the horizontal plane, another pyranometer is installed for measurements of global horizontal irradiance, and a sun tracker with pyrheliometer and pyranometer with shading assembly is installed for measurement of direct and diffuse irradiance. Aside from the irradiance sensors, a weather station is installed that measures ambient temperature, precipitation type and intensity, relative humidity and wind-speed and direction. A more detailed description of the measurement system is given in [5].

2.1.3. Data acquisition, filtering and analysis

The data from the different sensors is obtained at different frequencies. Weather and irradiance data and spectral data is measured at 30 second intervals. An IV curve is measured for all 23 installed PV modules in a series of measurements that starts every 2 min.

The data is processed in *LabVIEW* software [7] and subsequently stored in a *MySQL* database. During the processing in *LabVIEW* and before insertion in the *MySQL* database, several filtering steps are performed to flag PV measurements that do not fulfil several quality criteria: (i) stable irradiance during the measurement is ensured by checking irradiance before and after the measurement of an IV curve and flagging measurements with a deviation of more than 5%; and (ii) some snowy days have manually been flagged, because the partial snow cover causes irregular *I-V* curves, and/or incorrect irradiance measurements if the snow covers the pyranometers, and full snow cover of either pyranometers or PV modules also causes incorrect measurements.

In this study, we analyse the effect of different operation parameters on PV module performance. We do this by taking the complete dataset measured over the period of 2014 July through 2015 December, and filtering the data to investigate the effect of each parameter separately. For each parameter, we apply a filter that restricts the values of all other parameters to around their STC values. Hence, we filter data for irradiance, temperature, spectral irradiance, AOI and clear-sky index.[†] The range of each filter parameter is shown in Table II. To describe the performance effect of each parameter, we perform a fit of the selected data to a model (physical or general) that will describe the performance of the PV module as a function of the investigated parameter. We have used the Python programming language in conjunction with the *SciPy curve_fit* module [8] to process the data. The *curve_fit* module performs least-squares fitting of data using the *Levenberg-Marquardt* algorithm. The models used for fitting the different parameters, and our model optimisation approach are detailed in the next discussion.

2.2. Model optimisation with second iteration

The filter ranges discussed previously and shown in Table II were chosen to limit the variation to values around STC, except for the parameter currently investigated. However, in some cases, the filter ranges need to be broadened. For instance, for the analysis of AOI effects, filtering of irradiance and APE around STC values would exclude most of the AOI measurements greater than 15°. As a result of these broadened filter ranges, the effect of irradiance and APE could be reflected in the data – and resulting model fits – for AOI. Furthermore, even with datasets filtered more closely around STC, the effect of variations in the filtered parameters could still be present in the data and thus affect the resulting model fits. To account for this problem, we perform a second iteration of the model fitting, by correcting the raw data with the models obtained in the first model fit iteration. For example, for AOI, we correct the data using the models obtained for irradiance, temperature and APE, and perform a second model fit using this correct data. We assess the change in the quality of the fit by comparing the root-mean-square error of the model fit before and after the model optimisation.

2.3. Main performance functions

In this study, we analyse the effect of deviations from STC in terms of irradiance, module temperature, spectral

[†] Clear-sky index is calculated here as the ratio between measured direct normal irradiance and modelled clear-sky direct normal irradiance.

2017; **25**:218–232
DOI: 10.1002/pip

composition of irradiance and AOI. Although module performance is also affected by module stability [9], especially a-Si modules [10–12], and there is some evidence of module stability fluctuations in our dataset for a limited number of modules, we neglect this effect in our study, as we assume the amplitude of the effect of stability variation at our test site to be limited because the devices have been light-exposed for more than 1 year before the start of the dataset, and the effect of thermal annealing is likely limited at Northern-European locations [12,13].

We have fitted the datasets to models describing the PV module performance. From here on, we define performance as the instantaneous performance ratio *PR* or relative-to-STC power P_{rel}:

$$PR = P_{rel} = \frac{mP_{MPP}}{P_{STC}} \cdot \frac{1000\ \mathrm{W/m^2}}{G_{POA}} \tag{1}$$

where mP_{MPP} and P_{STC} are the measured and STC rated maximum power, respectively, and G_{POA} is the in-plane irradiance.

For irradiance and temperature, we have used physical models for fitting the data, however, in the case of spectral composition and AOI, we have used polynomial models based on the approach in [14]. In the following sections, we discuss the models used and their background. The effect of irradiance, temperature, APE and AOI is described by the factors f_{irr}, f_{temp}, f_{APE} and f_{AOI} respectively. These factors are detailed in the following sections.

2.3.1. Irradiance

The effect of irradiance on the power output of PV modules is almost linear and is very reasonably approximated by the function:

$$P_{MPP} = G_{POA} \cdot \frac{P_{STC}}{1000\ \mathrm{W/m^2}} \tag{2}$$

The short-circuit current increases linearly with irradiance, but in the one diode model for an ideal solar cell without shunt or series resistances, the open-circuit voltage (V_{oc}) increases logarithmically with irradiance:

$$V_{oc} = \frac{kT}{q} \ln\left(\frac{I_{sc}}{I_0} + 1\right) \tag{3}$$

where k is the Boltzmann constant, T the temperature, q the elementary charge, I_{sc} the short-circuit or light-generated current and I_0 the diode or dark saturation current. As irradiance decreases, I_{sc} decreases linearly, and the efficiency of the PV modules thus becomes lower because the decrease of V_{oc} with I_{sc}.

The efficiency as a function of light intensity is also affected by the shunt (R_{sh}) and series R_s) resistance in the solar cells and the PV module. As shown in the two-diode model [15], efficiency decreases at high light intensity because of the effect of series resistance and decreases at low light intensity due to the effect of shunt resistance:

$$\begin{aligned} I = I_{sc} &- I_{0_1}\left(\exp\left(\frac{V + IR_s}{kT}\right) - 1\right) \\ &- I_{0_2}\left(\exp\left(\frac{V + IR_s}{2kT}\right) - 1\right) \\ &- \frac{V + IR_s}{R_{sh}} \end{aligned} \tag{4}$$

where I_{0_1} and I_{0_2} are the diode saturation currents for the two diodes. In practical operating conditions, the combined effect of V_{oc}, R_s and R_{sh} on module output power means that in most cases, the relation between irradiance and power is linear, but at low light (below 200–300 W/m^2), the P_{mpp} deviates from this linear relation [16,17]. Various models exist to describe this behaviour, here, we follow the example of Dirnberger *et al.* [18] by using the model from Heydenrich *et al.* [19] as it was found to accurately describe low-light behaviour of the PV modules considered here [18]:

$$f_{irr} = PR(G) = aG + b\ln(G+1) + c\left(\frac{\ln^2(G+e)}{G+1} - 1\right) \tag{5}$$

where f_{irr} is a factor describing the change in *PR* as a function of irradiance, a, b and c are empirical parameters that describe the low-light behaviour of the PV modules, and e is Euler's number. We have adjusted the model to fit performance ratio *PR* as a function of irradiance, instead of efficiency. To analyse the effect of irradiance on *PR* and energy yield and establish these parameters, we have selected measurements from our dataset with a BOM temperature within 4.5°C from STC (25°C), an APE between 1.848 and 1.904 eV, and an AOI below 57°, which was found to be a 'critical' angle for AOI effects [20]. As mentioned before, we aim to filter data around STC conditions and vary only the investigated parameter. To obtain a full range of irradiance measurements between 0 and 1500 W/m^2 however, we need to include measurements at high diffusivity. Therefore, we have not used clear sky index as a filter parameter in this case.

2.3.2. Temperature

Another parameter influencing the performance of PV modules is temperature. As the temperature of PV cells increases, the open-circuit voltage decreases because of temperature dependence of the dark saturation current I_0, as is shown in this derivation of the single diode equation (Equation 3) for an ideal diode: As I_0 is a function of the intrinsic carrier concentration, which in turn is a function of temperature, it can be expressed as follows:

$$I_0 = CT^3 \exp\left(-\frac{E_{g0}}{kT}\right) \tag{6}$$

where C is a temperature-independent constant, and E_{g0} is the band gap of the material, extrapolated to absolute zero temperature. As can be seen in the Equations (3) and (6), the term T in the exponent of Equation (6) makes

DOI: 10.1002/pip

that the temperature dependence of I_0 has more effect on V_{OC} than the term T outside of the natural logarithm in Equation (3) and thus the result is a negative dependence of V_{OC} on temperature. Also shown in (3) is that the temperature dependence of a PV module is as related to the band gap of the used material. Generally speaking, the effect of temperature on PV module performance decreases with the band gap of the material. High band gap technologies, such as a-Si and CdTe thus have lower specified temperature coefficients than crystalline silicon and CI(G)S PV modules. We have in this study assumed a linear relation between temperature and performance:

$$f_{\text{temp}} = PR(T) = 1 + (T_{\text{BOM}} - 25) \times \gamma_{P\text{rel}} \tag{7}$$

where f_{temp} is a factor describing the change in PR as a function of temperature, T_{BOM} is the BOM temperature and $\gamma_{P\text{rel}}$ is the STC temperature coefficient of P_{rel} (which is equal to the temperature coefficient of P_{mpp}). As shown in Table II, we have selected data from an irradiance range from 950–1050 W/m^2, with a clear sky index between 0.9 and 1.1 and APE within 1% of STC. The used fit model thus corrects power for irradiance assuming them to be linearly proportional in the considered irradiance range.

2.3.3. Spectrally distributed irradiance

The STC conditions at which PV modules are rated also prescribe the spectral composition of the light source used to determine STC power output of the module. The spectral distribution should conform to the AM 1.5 G standard solar spectrum as defined by IEC 60904-3 ed. 2 [21]. For the wavelength range of the spectroradiometer used in this study (350–1050 nm), the AM1.5 APE is 1.876 eV. The effect of spectral variation on PV device performance is a result of multiple factors: (i) the band gap of the material used for the PV module determines a minimum photon energy that can generate free carriers in the PV cells, (ii) above this threshold, the absorption of and carrier generation by photons varies as a function of their wavelength. (iii) the energy in photons above the band gap threshold is not converted into current but rather dissipated as heat in the PV cells.

The effect of these parameters is reflected in Figure 1, which shows examples of the internal quantum efficiency (IQE) and spectral response (SR) of various types of PV modules. The IQE shows the relative amount of carriers generated for each photon wavelength (energy). The SR shows the resulting current generated per watt of irradiance at each photon wavelength. The SR is calculated by multiplying the IQE with the ratio of the band gap to the photon energy. Spectral shifts towards the red region of the spectrum (low photon energy, large wavelength) usually result in lower generated current, as more photons are below the band gap threshold, and thus the IQE and SR are lower. The effect of spectral variation on PV device performance is thus most pronounced for technologies with a narrow SR, such as CdTe and a-Si. Especially for a-Si, there is much evidence in the literature of this effect

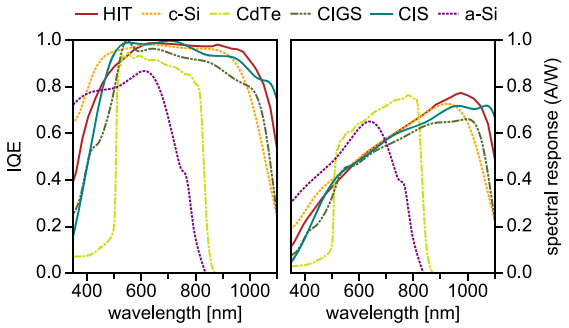

Figure 1. Illustrative example of the internal quantum efficiency (IQE) and spectral response of six different photovoltaic cell technologies. Data courtesy of [22] and [23]. [Color figure can be viewed at wileyonlinelibrary.com.]

[9,24–30]. As two-dimensional data, the measured spectra are an inconvenient way to present the effect of spectral variation on PV performance. Therefore, researchers often analyse the performance of PV as a function of a one-dimensional parameter representing the spectra. Examples are the useful fraction [31–33], the spectral factor or spectral mismatch factor (MMF) [9,24,25,34] and the APE [4,34,35]. The useful fraction, spectral factor and spectral mismatch factor require that a researcher knows the SR of the PV module under study. This data is not available publicly for commercial PV modules. In contrast, the APE is an external parameter, as it represents the average energy of an incoming photon. It is calculated as follows:

$$APE = \frac{\int_a^b E(\lambda)d\lambda}{q\int_a^b \phi(\lambda)d\lambda} \tag{8}$$

where $E(\lambda)$ is the photon energy, $\phi(\lambda)$ is the photon flux at wavelength λ, and a and b are the limits of integration, which are 350 and 1050 nm for the spectroradiometer used in this analysis. A number of studies have confirmed the applicability of APE as an indicator of unique spectra [36–40]. The APE varies both on a daily and seasonal basis, due to increased airmass at sunrise and sunset compared to noon, and in winter compared with summer. For instance, before sunrise and after sunset, as there is only diffuse light from the atmosphere, the spectral irradiance is blue-shifted and APE is high. When the sun is close to the horizon, the light is red-shifted and APE is low. During the day APE increases again to a maximum around noon. As the sun has a lower zenith at noon in winter compared with summer, the APE is lower in winter compared with summer months. Furthermore parameters like cloud cover, atmospheric water and aerosol content affect APE by absorption and scattering of solar insolation.

For limited ranges of APE values, and for some PV module types the effect of APE on performance seems to be linear. However, considering a full range of APE measurements, the relation is non-linear. Here, we have used the approach described by [14] for airmass and AOI

2017; **25**:218–232
DOI: 10.1002/pip

effects, which is to use an empirical polynomial model to fit the data. As variations in the spectrum affect the power output indirectly, but current generation directly, we have analysed performance in terms of the normalised short-circuit current, nI_{sc}:

$$nI_{sc} = \frac{mI_{sc} \cdot (1 + \alpha_{I_{sc}} \cdot (T_{BOM} - 25))^{-1}}{G_{POA} \cdot (G_{STC})^{-1} \cdot rI_{sc}} \quad (9)$$

where mI_{sc} and rI_{sc} are the measured and STC rated short-circuit current, and $\alpha_{I_{sc}}$ is the temperature coefficient of short-circuit current. As shown in this equation, we use the module specifications to correct the measured short-circuit current for temperature, as the temperature coefficients obtained with the analysis of section 2.3.2 refer to those for module power and thus cannot be used to correct the data for measured short-circuit current. We fitted data for the performance ratio of the short-circuit current to a polynomial model:

$$f_{APE} = PR(APE) = a_0 + a_1 \cdot APE + a_2 \cdot APE^2 + a_3 \cdot APE^3 + a_4 \cdot APE^4 + a_5 \cdot APE^5 \quad (10)$$

where f_{APE} is a factor describing the change in *PR* as a function of APE, a_n are a set of empirical parameters, *APE* is the measured APE value and f_{APE} is the relative effect on performance.

2.3.4. Angle-of-incidence

The STC power ratings of PV modules are performed with a beam of light that is perpendicular to the PV modules surface. As a consequence of the (apparent) movement of the sun across the Earth's sky, the sun's light hits the PV modules at different angles throughout the day, as solar zenith and azimuth change. Because of the Earth's inclination, there is also a strong seasonal variation in the course of zenith and azimuth throughout the day. Combining the solar zenith, azimuth, and the slope and orientation of the PV module, we can calculate the AOI between the beam component of solar irradiance and the PV module surface. In Twidell and Weir [41], it is defined as follows:

$$\cos\theta = \cos\theta_z \cdot \cos\beta + \sin\theta_z \cdot \sin\beta \cdot \cos(\phi_s - \phi) \quad (11)$$

where θ is the AOI, θ_z is the solar zenith, β is the PV module slope, ϕ_s is the solar azimuth and ϕ is the orientation of the PV modules (by definition $\phi = 0$ for a panel oriented to the south in the northern hemisphere).

A higher AOI results in a decrease of light coupled into the PV cells [20,42–44]. To analyse the effect of AOI on the performance of the PV modules we have fitted a polynomial model from [14] to the data:

$$f_{AOI} = PR(AOI) = a_0 + a_1 \cdot AOI + a_2 \cdot AOI^2 + a_3 \cdot AOI^3 + a_4 \cdot AOI^4 + a_5 \cdot AOI^5 \quad (12)$$

where f_{AOI} is a factor describing the change in *PR* as a function of AOI, a_n are a set of empirical parameters and *AOI* is the AOI. The filter ranges were adjusted to allow for a larger range of APE values and lower irradiance measurements, as STC values for irradiance and APE are generally only measured at very low angles-of-incidence. Previous research suggests a strong decline in performance at high angles-of-incidence [45–47], mainly (after correcting for irradiance) because of increased reflectance at high angles-of-incidence [46].

2.4. Seasonal and annual effect of parameters

The fit models obtained are used to calculate the effect of each parameter on module performance, for all the measurements in the complete dataset and for the complete period. This allows us to track the effects over time and to analyse the contribution of each parameter to seasonal and annual energy yield.

To combine both the variation in operating conditions and the effect of these variations on PV performance, we analyse and plot the performance deviation as a function of the percentile of data measured for each parameter. This allows us to visualise, for instance, that although the effect of temperature on performance is very pronounced, the resulting variation in performance, taking into account a full year of module temperature variation, is low, as the majority of measurements have temperatures around STC values, much lower than NOCT, because of an exceptionally large amount of low-irradiance measurements (section 3 and Figure 2).

The calculated parameter effects also allow us to show the seasonal variation of performance as a result of the variation in operating conditions. We aggregate this data per 4 weeks and use weighting so the graphs show the effect on energy yield. For irradiance, temperature and APE we use in-plane irradiance for weighting, for AOI, we use direct irradiance (as we have many measurements with high levels of diffuse irradiance). We also analyse the effect on an annual basis in a similar way, but aggregating all data for 1 year.

3. CHARACTERISATION OF OPERATING CONDITIONS

Figures 2 and 3 show the characterisation of weather conditions at the UPOT. Data for irradiance, APE, ambient and module temperature and AOI show that realistic operating conditions for a North-Western European location hardly ever agree with STC, especially for irradiance and AOI.

In our location, module temperature is almost normally distributed around STC (25°C), although the variance is quite large. This is striking as the nominal operating temperature is between 40 – 50°C for the studied modules. However, our location is characterised by large amounts of low irradiance measurements, well below the 800 W/m^2 at

DOI: 10.1002/pip

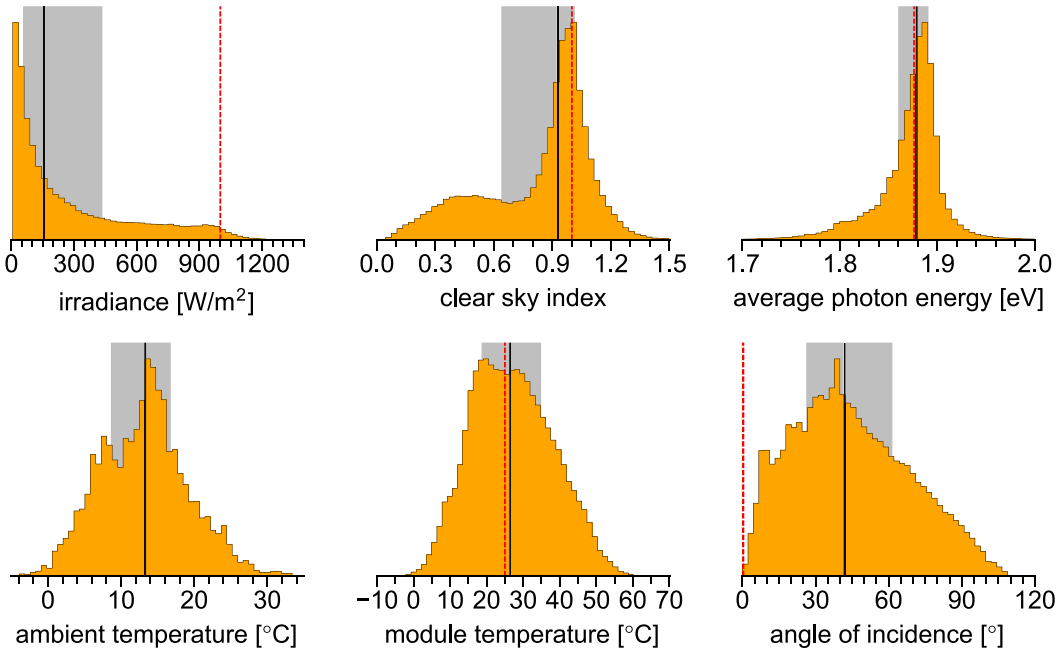

Figure 2. Distribution of irradiance, clear sky index, average photon energy, ambient temperature, module temperature (back-of-module temperature T_{BOM}) and angle-of-incidence at the Utrecht Photovoltaic Outdoor Test facility in Utrecht, the Netherlands, for the year 2015. The y-axis shows the relative probability of occurrence. Clear sky index, average photon energy, were weighted by irradiance, T_{BOM} by module power and angle-of-incidence by direct irradiance. Dashed red lines indicate standard testing conditions. Shaded areas indicate the interquartile ranges, the solid black lines the medians. [Color figure can be viewed at wileyonlinelibrary.com.]

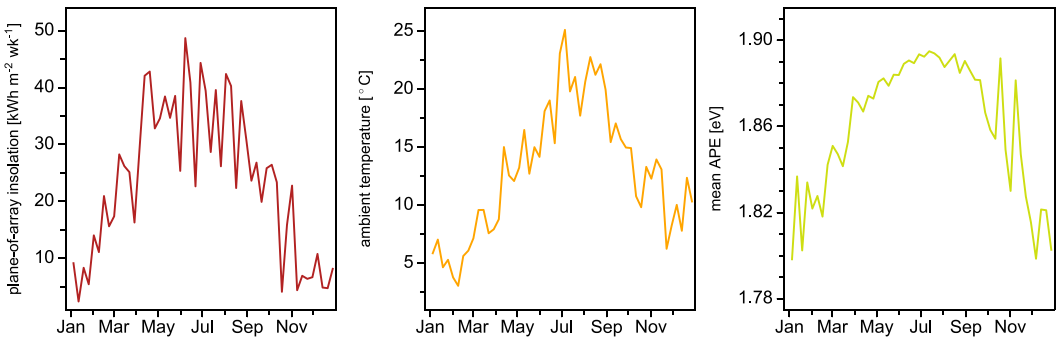

Figure 3. Weekly insolation (H_{POA}), mean temperature (T_{ambient}) and mean average photon energy at the Utrecht Photovoltaic Outdoor Test facility in Utrecht, the Netherlands, for the year 2015. Ambient temperature and APE where weighted by irradiance. [Color figure can be viewed at wileyonlinelibrary.com.]

which NOCT is established, with concurrently low operating temperatures. The distribution of APE is more or less around STC, but with very long tails, especially on the lower side. Almost no measurements have an STC AOI, and almost 98% of measurements have an irradiance lower than 1000 W/m^2. The development of insolation, mean air temperature and mean APE is shown in Figure 3. This figure shows that there is a very strong seasonal variation of all three parameters. It shows that only a small portion of the APE measurements are around STC.

These results indicate that for the location investigated, practically all measurements deviate significantly from STC, and as a result, the performance of PV modules could very well be significantly affected, especially on a seasonal basis. In the following sections, we investigate the effect of variation in irradiance, APE, module temperature and AOI on the performance of different types of PV modules.

4. MODEL FIT QUALITY

Table III shows the results of the initial model fits, and the model optimisation, which corrects the initial fit for each parameter, with the fit models from the other parameters (section 2.2). The table shows the root-mean-square error (RMSE) of the data to the models, for each module

2017; **25**:218–232
DOI: 10.1002/pip

Table III. Overview of root-mean-square errors (RMSE) of the model fit to the data for four parameters and eight devices. For each parameter, the top row indicates RMSE before, while the lower row indicates RMSE after optimisation and correction. Font style and colours are used as a visual aid to indicate improvement (bold, green) or deterioration (italics, orange) of the fit.

	Device							
Parameter	**H1** (%)	**M1** (%)	**P1** (%)	**P2** (%)	**A1** (%)	**CT1** (%)	**CG1** (%)	**CS1** (%)
Irradiance	2.85	3.28	4.87	3.08	3.43	3.52	3.32	4.10
	2.48	**2.50**	**2.80**	**2.65**	**2.11**	**2.75**	**3.11**	**3.66**
Temperature	1.02	0.93	2.34	0.91	1.57	1.35	1.49	1.39
	0.99	**0.80**	**0.97**	*0.94*	**1.00**	**1.23**	*1.50*	*1.47*
APE	1.03	1.05	1.26	1.10	1.15	1.59	1.42	1.26
	1.03	**1.01**	*1.27*	*1.11*	**1.06**	**1.50**	*1.49*	*1.29*
Angle-of-incidence	2.69	3.23	3.25	3.15	2.12	2.98	4.25	4.11
	1.21	**1.75**	**1.84**	**1.61**	**1.11**	**1.34**	**1.54**	**1.22**

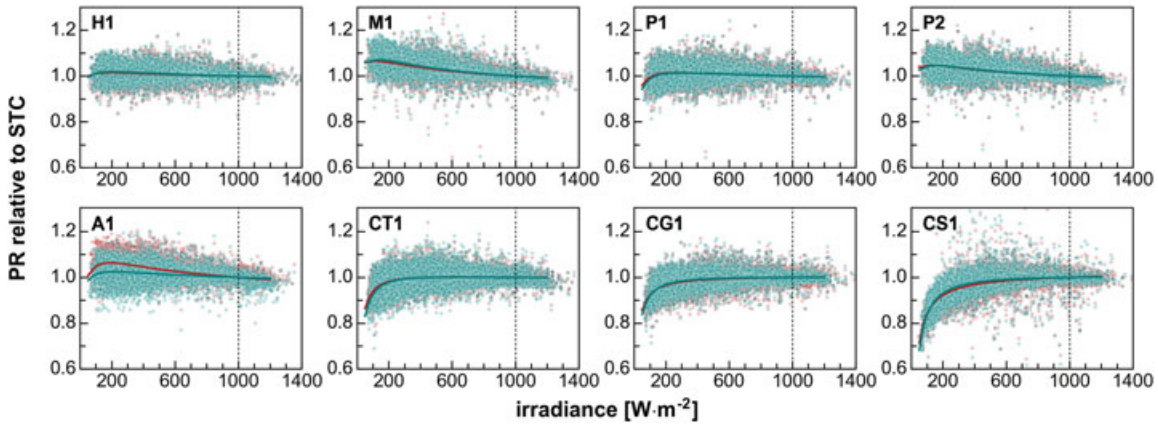

Figure 4. Performance ratio relative to standard testing conditions conditions as a function of irradiance, for eight different modules. Module names are indicated in the top left corner of the plots and refer to section 2.1.1 and Table I. The graphs show the non-linear model of Equation 5 fitted to the measured data. The red datapoints and curve indicate the raw data and fitted model, the blue datapoints and curve are the corrected data and optimised fitted model. Most red datapoints are not visible as they are plotted behind the blue ones. The dashed vertical line indicates STC irradiance. [Color figure can be viewed at wileyonlinelibrary.com.]

separately. The largest errors in the initial fit are found for irradiance and AOI. For temperature and APE, the RMSE is around 1% for most modules, while for irradiance and AOI, the error is around 3% but up to almost 5%. In most cases, the model optimisation improves the fit of the models. Notable exceptions are the P2, CG1 and CS1 modules, which show a deterioration for the fits in half or more of the cases. The most notable improvements of the fitted model occurs for the AOI fits.

5. MODULE PERFORMANCE

5.1. Irradiance

To analyse the effect of variation in irradiance intensity on PV performance, we have filtered data around STC conditions, varying only the irradiance in the range of 50–1400 W/m^2 (Table II). Because of the high time resolution of the measurement, the datasets include a significant number of irradiance measurements well above 1000 W/m^2, because of cloud-induced super-irradiance. The results of the analysis are shown in Figure 4. The selected data were used to fit the model of Equation 5. For four types of modules, we find that deviation away from STC irradiance leads to a small increase of performance (H1, M1, P2, A1) relative to STC conditions. Below approximately 175–200 W/m^2 however, performance of these modules starts to deteriorate. Contrary, for module P1 we do not see the performance increase, likely because of a lower series resistance in this module. For the CdTe and CI(G)S modules, lowered performance is measured at lower irradiance values. Especially for the CIS module this effect seems very pronounced. These results are striking, considering that it is often reported that thin-film modules operate better at low light conditions compared to crystalline silicon modules. The strong decrease of performance could be due to a relatively low shunt resistance in the modules [48], as the adverse effect of low shunt resistance on performance is greater as irradiance is lower.

DOI: 10.1002/pip

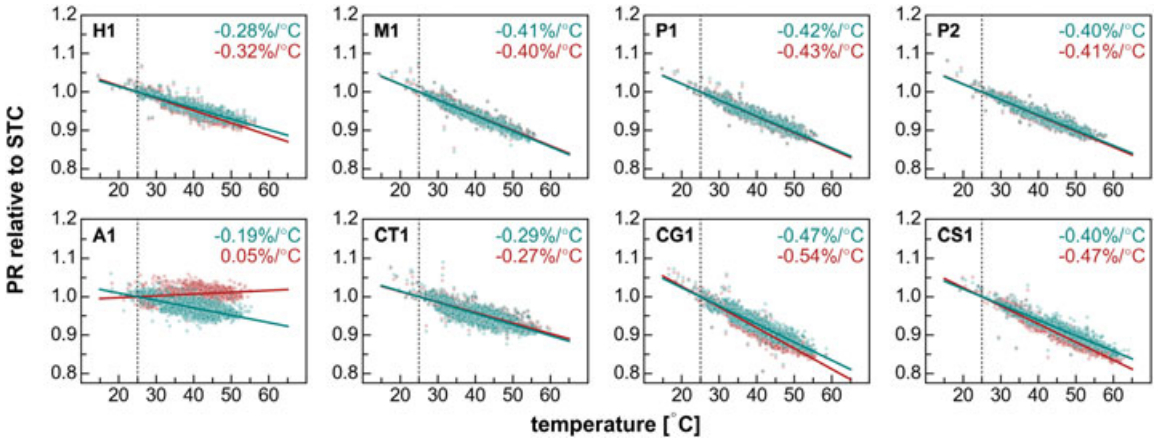

Figure 5. Performance ratio relative to standard testing conditions as a function of back-of-module temperature, for eight different photovoltaics modules. Linear models were fitted to the data (solid red and blue lines). The red datapoints and lines indicate the raw data and fitted model, the blue datapoints and lines are the corrected data and optimised fitted model. The temperature coefficient of module power is shown in the top right corner for raw and corrected data. The dashed vertical line indicates standard testing conditions temperature. [Color figure can be viewed at wileyonlinelibrary.com.]

The results show that the filtering still results in large datasets with a large spread around the model fits. As a result, compared to the analyses for other parameters, the fit errors (RMSE) are relatively high. The model optimisation decreases the fit errors, however the effect on the data and the fits is not as visible in Figure 4.

5.2. Temperature

The effect of temperature on PV module performance was estimated by filtering data around STC irradiance, APE and AOI and varying only BOM temperature. For the filter ranges see Table II. The results of our analysis, shown in Figure 5, indicate for each module type the temperature coefficient at maximum power.

The values obtained from this outdoor, long term measurement mostly agree quite reasonably with those reported by the manufacturer in the module specification sheets. Notable exceptions are the A1, CS1 and CG1 modules. The thin-film a-Si/a-Si tandem A1 module shows a temperature coefficient of +0.05%/K for raw data, while module specifications indicate a negative coefficient of –0.20%. After the model optimisation however, the fit is shifted towards a value of –0.19%, which is very close to the module specifications. The positive value obtained for raw results is predominantly caused by variation in spectral irradiance, which have quite a strong effect on the performance of this module (section 5.3). The importance of considering the spectrum for outdoor determination was also shown by Makrides *et al.* [49].

For the CS1 and CG1 (CIS and CIGS) modules, we observe a much stronger negative coefficient of maximum power (–0.54%/K and –0.47%) for raw data, than in the module specifications (–0.45% and –0.39%). After correction, the coefficients are –0.47%/K and –0.40%/K, and the difference with module specifications is 0.07%/K smaller for both modules, mainly due to correction for APE and irradiance. From the results we can also observe that the CS1 module seems to operate at higher temperatures compared to the other modules investigated, even though the specified NOCT does not indicate this. For the CT1 module, the difference in fitted and specified coefficient is not very big for the raw data, but is bigger for the corrected data. This is likely an overcorrection for APE or the results of a temperature mismatch between BOM and cell.

The values obtained for the M1, P1 and P2 modules are quite close, but somewhat smaller (less negative) compared with the specified values. The data fitting indicate that each module seems 0.01%/K less affected by temperature change than the module specifications show, however, this difference is likely within the margin of error. The effect of data correction and model optimisation is small for these modules. The coefficient obtained for the H1 module is also close to module specifications, but is larger in the raw data, and smaller in the corrected data. This might be due to an overcorrection of the data.

5.3. Spectral variation

The effect of spectral variation (here analysed by means of APE) on the performance of the eight investigated PV modules is shown in Figure 6. The figure shows data measured at manually selected clear sky days, and a polynomial model fitted to this data. The results indicate as expected a strong effect of varying APE on the performance of the A1 (a-Si/a-Si tandem) module, while the effect is limited for crystalline silicon based modules (M1, P1, P2) and the H1 (heterojunction) module. In the low end of APE values, the CT1 module shows lowered performance, although the number of datapoints in this region is very small. Very low APE values are normally measured at high airmass and thus (for these fixed tilt modules) high

 Progress in Photovoltaics: Research and Applications published by John Wiley & Sons Ltd. 2017; **25**:218–232
DOI: 10.1002/pip

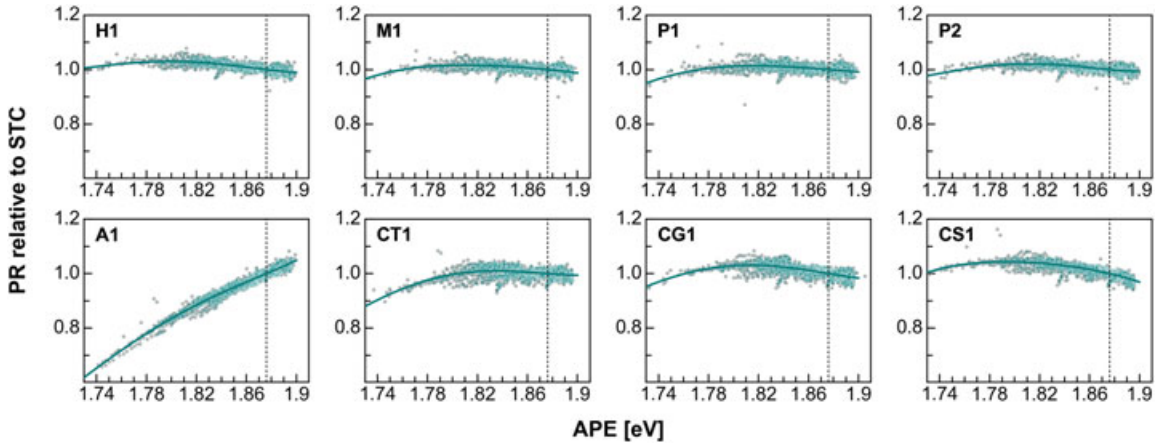

Figure 6. Performance ratio or short circuit current relative to standard testing conditions as a function of average photon energy (APE), for eight different photovoltaics modules. Polynomial models were fitted to the data (solid red and blue lines). The blue datapoints and curves are the corrected data and optimised fitted model. The dashed vertical line indicates standard testing conditions APE. Although the plots contain the raw data like Figures 4, 5 and 7, this data is obscured by the corrected data after correction as the effect of the correction is minimal. [Color figure can be viewed at wileyonlinelibrary.com.]

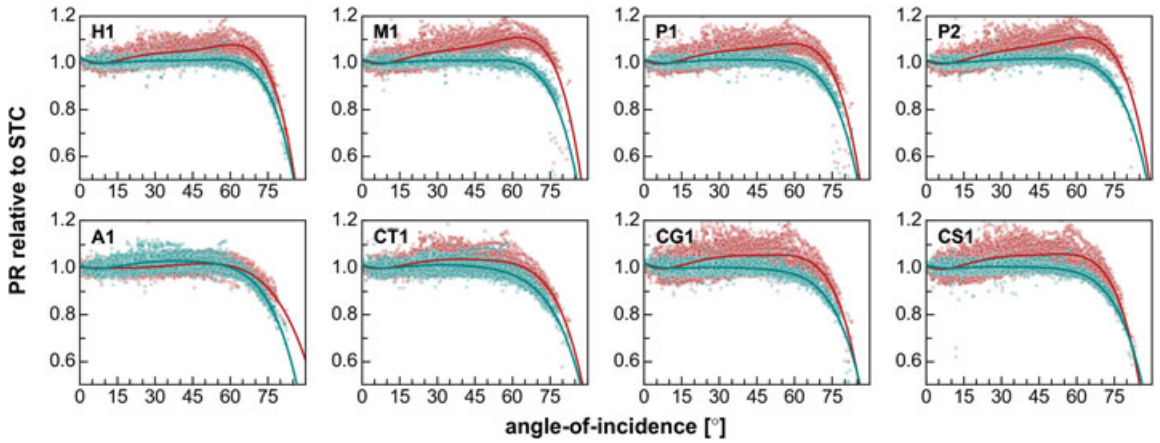

Figure 7. Performance ratio relative to standard testing conditions as a function of angle-of-incidence, for eight different photovoltaics modules. Polynomial models were fitted to the data (solid red and blue lines). The red datapoints and line indicate the raw data and fitted model, the blue datapoints and line are the corrected data and optimised fitted model. [Color figure can be viewed at wileyonlinelibrary.com.]

angles of incidence. However, these datapoints are filtered from the data for this analysis to avoid the data representing the effect of both parameters on PV module performance. For the crystalline silicon based modules (H1, M1, P1, P2) and the CI(G)S modules (CG1 and CS1) we observe a slight decrease of performance as the APE increases. This is likely related to the low band gap and the peak of SR at long wavelengths (Figure 1). At very low APE values, we do however observe a slightly decreased performance for these modules. For the CI(G)S modules this effect is stronger compared the crystalline silicon based modules. The model optimisation does not seem to affect the model fits. For all modules except the A1 module, the peak of performance is at a lower APE than STC conditions specify.

5.4. Angle-of-incidence

Figure 7 shows the effect of angle-of-incidence on the performance of the studied PV modules. The red and blue lines indicate the polynomial model fitted to the data (Equation 12). For all modules investigated, there is a strong decrease in performance at high angles of incidence, although the magnitude of the effect slightly differs from on module to the other. The effects of high angles-of-incidence do not necessarily depend on the semiconductor material in the module, but likely more on the optical structure of the whole device, and as such the type of glass used as front cover of the module, and the applied laminate [46]. This seems to be confirmed by our results, which distinguish the modules with a smooth glass front cover (CT1,

DOI: 10.1002/pip

CG1 and CS1) from the textured glass modules (H1, M1, P1, P2). In the latter case, the onset of angular losses is at a higher AOI, but the decline is sharper, compared with the more gradual effect observed in the smooth glass modules. The fit for the A1 module seems affected by a large spread in both the raw and uncorrected data.

The data correction and model optimisation substantially affects the data and resulting model fits. The raw data and their fits clearly exhibit the effect of low irradiance and low temperature, at high angles of incidence. Correction for these parameters, and APE, significantly improves the model fit for all modules investigated (Table III). For the crystalline silicon based modules M1 and P2, we clearly observe enhanced performance at low irradiance levels that coincide with large angles of incidence. This is visible at the 'knee' of the graphs in Figure 7. As a result of the model optimisation, this effect is reduced significantly, and the graphs become nearly horizontal up to roughly 60°. For the CG1 and CS1 modules, an opposite effect is observed, where the correction for low performance at low irradiance shifts the AOI fit and data to the right (Figure 7).

5.5. Module comparison

Figures 8 and 9 show a comparison of the effects of the investigated parameters for the eight investigated PV modules. Figure 8 shows the fitted models from Figures 4–7. In this figure, we can clearly see that: (i) low irradiance most substantially affects the performance of the CS1 module, but the CG1 and CT1 modules also show strongly decreased performance at low irradiance conditions, contrary to what is often reported for CI(G)S

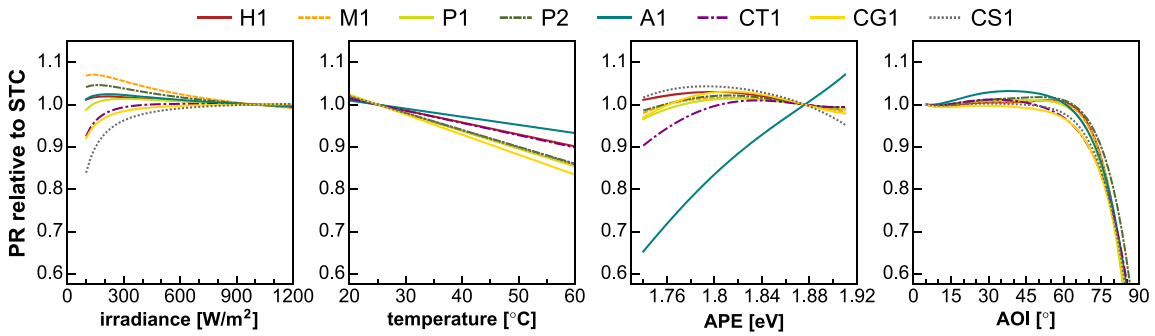

Figure 8. Comparison of Performance Ratio (relative to STC) of eight PV modules as a function of irradiance, temperature, average photon energy (APE) and angle-of-incidence. [Color figure can be viewed at wileyonlinelibrary.com.]

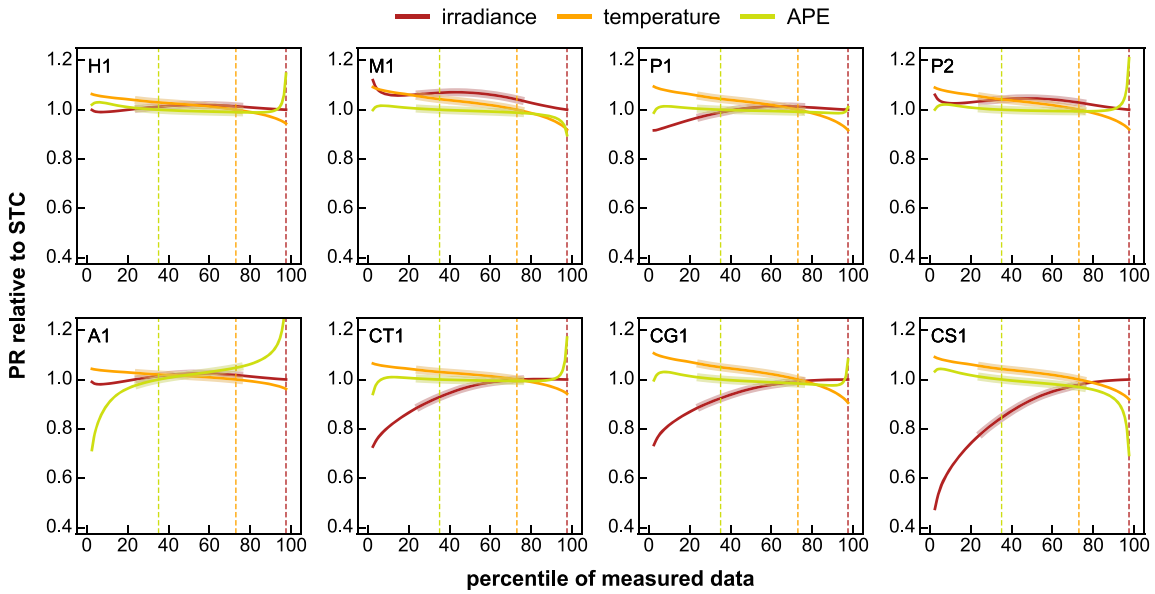

Figure 9. Comparison of Performance Ratio (relative-to-standard testing conditions) of eight photovoltaics modules as a function of the measured percentiles for irradiance, temperature and average photon energy (APE). The interquartile range is indicated by the thicker portion of the lines. The dashed vertical lines shows the percentile location of standard testing conditions for each parameter. Angle-of-incidence is omitted from this figure, as its effect on overall performance is also affected by the fraction of direct light. [Color figure can be viewed at wileyonlinelibrary.com.]

2017; **25**:218–232
DOI: 10.1002/pip

modules. The performance increases at low irradiance for the P2 and especially the M1 module; (ii) increased module temperature has the most effect on the CG1 module (–0.47%/°C), slightly less for the M1, P1, P2 and CS1 modules (–0.40 to –0.42%/°C), and significantly less for the H1 (–0.28%/°C), CT1 (–0.29%/°C) module and A1 (–0.20%/°C) module; (iii) the effect of spectral variation is very pronounced for the A1 module, and most limited for the crystalline silicon based modules; (iv) the AOI losses are significant for all modules, but the effect is different for smooth glass modules (CT1, CG1, CS1) compared with textured glass modules (H1, M1, P1, P2). The fit for the A1 module seems negatively affected by noise in the data.

Figure 9 combines the fitted models from Figures 4–7 and the measurements presented in Figure 2. It shows the performance deviation as resulting from variation of the four investigated parameters as a function of the relative occurrence of the variation in each parameter. The dashed vertical lines indicate the location of STC values for each parameter. The figure makes visible that for some modules, the observed variation in operating conditions does not result in strong deviation of performance relative to STC. This is true mainly for H1 and P2, and to a lesser extent for M1 and P1. Especially for the CS1 module, but also for the CG1 and CT1 modules, strong deviation from STC performance is observed as a result of observed variation, mainly irradiance and temperature. The effect of observed variation in spectral composition of irradiance is especially clear for the A1 (a-Si/-a-Si tandem) module, because the optimal current matching between the two cells in the tandem module is affected as the APE shifts away from STC conditions [38,50]. Thus, this effect does not so much depend on the module material, but rather on the tandem structure.

6. EFFECT ON SEASONAL AND ANNUAL ENERGY YIELD

We have analysed the effects of observed variation in operation conditions on both seasonal and annual performance. The results of this analysis are shown in Figures 10 and 11. Figure 10b shows that especially variation in module temperature leads to a substantial seasonal variation in performance for all modules, although the effect is of course smaller for the modules with lower temperature coefficients. Because of high operating temperatures, performance is decreased in summer. In winter, module temperatures are so low performance is increased above STC values (although energy yield in this period is low due to low insolation). Variation in APE also results in seasonal variation of performance, especially for the A1 module, showing a peak in summer (high APE) and strongly decreased performance in winter (low APE) in Figure 10c. Low APE values observed in winter can lower the performance of this module by almost 15%. For the (non-tandem) CT1 module this seasonal effect is similar but much less pronounced. Fig 10a shows that because of deviations in irradiance, some modules, most obviously the CS1 modules, operate at lower performance compared with STC year-round, while other modules, like the M1 module, benefit from year-round lower-than-STC irradiance. The effect of AOI on seasonal performance variation is small, as this effect is compensated by an increase of diffuse irradiance, and the majority of measurements performed have a high fraction of diffuse irradiance.

The contribution of observed variation in operating conditions to annual performance is shown in Figure 11. This figure indicates that for all modules there is a negative

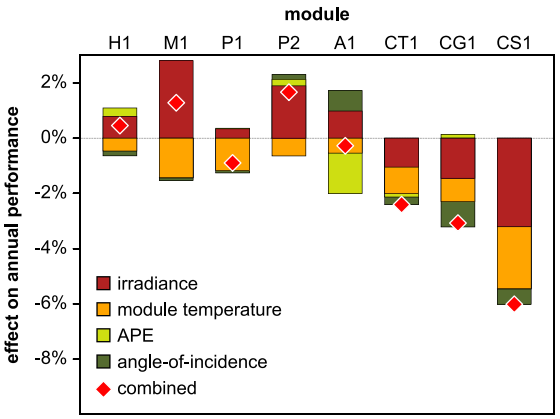

Figure 11. Stacked bar chart showing a comparison of the effects of variation in four parameters on annual module performance. The red diamonds indicate the combined effect of all four parameters. For the module specifications please refer to Table I. [Color figure can be viewed at wileyonlinelibrary.com.]

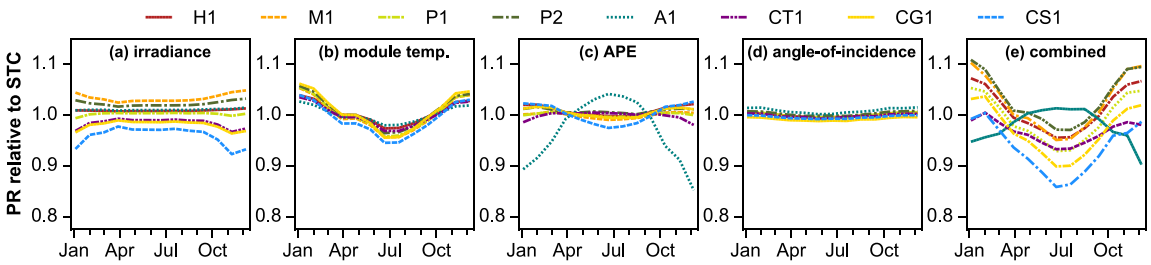

Figure 10. Overview of the effect of variation of four parameters, and their effects combined, on the seasonal performance of eight photovoltaics modules. For the module specifications refer to Table I. [Color figure can be viewed at wileyonlinelibrary.com.]

DOI: 10.1002/pip

effect of module temperature and AOI on annual performance, except for the A1 and P2 modules, that appear to get a small performance bonus from deviation of AOI values, which we cannot conclusively explain. For both modules the AOI models fitted show slightly (P2) or significantly (A1) increased performance between roughly 15° and 65°. For the A1 module, this might be due to increased absorption in the thin silicon film as a result of the longer trajectory of light in the absorbing layer. For the P2 module it seems outliers in the dataset (visible in Fig 7) could have affected the model fit.

Deviations of irradiance from STC conditions results in enhanced performance for five modules: H1, P1, P2, A1 and especially M1, while the other thin-film modules show poor low-light performance and thus are affected negatively by irradiance in terms of annual output.

Especially the CS1 module, which operates generally at higher temperatures compared with the other modules, temperature losses are large. This module is also very strongly affected by the low irradiance operating conditions, and AOI effects. On an annual basis, most modules are (almost) unaffected by variations in spectral composition of irradiance. The one exception is the thin-film a-Si/a-Si tandem A1 module.

7. CONCLUSIONS

We have characterised and compared the performance of different types of PV modules, under realistic operating conditions observed in a North-Western European installation location, in the context of an R&D project focussing on the development and assessment of silicon heterojunction (SHJ) technology. We have analysed the effect of deviations from STC observed for irradiance, module temperature, spectral composition of irradiance and AOI. Our results show that the effect of observed variations in operating conditions affect modules very differently according to module type (semiconductor material) but also the materials used in the modules, such as the type of glass used in the front cover of the module.

In our study, a CIS was most affected by variations of operating conditions. This module exhibited, on an annual basis, a negative effect of variations in all investigated parameters, and an especially strong effect of irradiance and temperature variations on annual performance. The combined effect of all parameters was a decrease in annual energy yield of more than 6%, of which 3.2% caused by low irradiance and 2.2% by high temperature operation of the module. AOI effects amounted to a performance loss of around 0.5%. The other modules investigated were much less affected by variations in operating conditions, with the annual combined effect ranging from –3.1% to +1.6%.

Focusing on the SHJ module, our results show that this module performs very similar to other crystalline silicon based modules in the study. The benefit of SHJ's small temperature dependence is confirmed by lower temperature related losses, and there is no substantial difference in the response to varying spectral conditions.

Examining the effects in the context of PV module types (semiconductor materials), we see that not only all effects seem to be related to semiconductor material but also to the type of glass on the front of the module, and other module parameters, such as a tandem or single junction structure, or the packaging in the module (warm or cool packaging).

By supplying more information on the effect on PV module performance of different operating parameters, like spectral irradiance, low irradiance conditions and AOI, PV producers could improve the estimates installers make on the expected energy yield of the PV systems they install, especially when they can connect this with data on local operating conditions. We argue that the addition to the module datasheets of SR data, and data showing the performance of the modules as a function of irradiance and AOI would improve the estimates of installers substantially.

Acknowledgement

This research was funded by Stichting Technologische Wetenschappen within the FLASH Perspectief programme under project number 12172.

REFERENCES

1. IEA PVPS. Trends 2015 in Photovoltaic Applications. *IEA-PVPS T1-27:2015*, International Energy Agency, 2015.
2. Panasonic. *Panasonic HIT™*, 2016. http://panasonic.net/ecosolutions/solar/hit/.
3. ASTM I. ASTM E2848-13, Standard Test Method for Reporting Photovoltaic Non-Concentrator System Performance, ASTM International, West Conshohocken, PA, 2013.
4. Betts TR, Jardine CN, Gottschalg R, Infield DG, Lane K. Impact of spectral effects on the electrical parameters of multijunction amorphous silicon cells, In *Proceedings of 3rd World Conference on Photovoltaic Energy Conversion, 2003*, 2003; 1756–1759.
5. van Sark WGJHM, Louwen A, de Waal AC, Schropp REI. UPOT: The Utrecht photovoltaic outdoor test facility, In *Proceedings of the 27th European Photovoltaic Solar Energy Conference and Exhibition*, WIP Renewable Energies, Aachen, Germany, Frankfurt, Germany, 2012; 3247 – 3249.
6. EKO Instruments. *MP-160 I-V Tracer*, 2016. http://eko-eu.com/products/photovoltaic-evaluation-systems/i-v-tracers/mp-160-i-v-tracer.
7. National Instruments. *LabVIEW*, 2010.
8. The SciPy community. *Scipy.optimize.curve_fit*, 2016. http://docs.scipy.org/doc/scipy/reference/generated/scipy.optimize.curve_fit.html.
9. Dirnberger D, Blackburn G, Müller B, Reise C. On the impact of solar spectral irradiance on the yield of

DOI: 10.1002/pip

different PV technologies. *Solar Energy Materials and Solar Cells* 2015; **132**: 431–442.
10. Fanni L, Virtuani A, Chianese D. A detailed analysis of gains and losses of a fully-integrated flat roof amorphous silicon photovoltaic plant. *Solar Energy* 2011; **85**(9): 2360–2373.
11. Virtuani A, Fanni L. Seasonal power fluctuations of amorphous silicon thin-film solar modules: distinguishing between different contributions: seasonal power fluctuations of a-Si thin-film solar modules. *Progress in Photovoltaics: Research and Applications* 2014; **22**(2): 208–217.
12. Skoczek A, Virtuani A, Cebecauer T, Chianese D. *Energy yield prediction of amorphous silicon PV modules using full time data series of irradiance and temperature for different geographical locations*, 2011.
13. Virtuani A, Skoczek A, Strepparava D. *Modeling the performance of amorphous silicon photovoltaic modules in different geographical locations in Europe*, 2014.
14. King DL, Boyson WE, Kratochvill JA. Photovoltaic Array Performance Model. *SAND2004-3535*, Sandia National Laboratories, Albuquerque, New Mexico, USA, 2004.
15. Markvart T, Castañer L (eds.) *Practical Handbook of Photovoltaics: Fundamentals and Applications*, Repr. Elsevier: Oxford, 2003. OCLC: 179994435.
16. Reich NH, van Sark WGJHM, Alsema EA, Lof RW, Schropp REI, Sinke WC, Turkenburg WC. Crystalline silicon cell performance at low light intensities. *Solar Energy Materials and Solar Cells* 2009; **93**(9): 1471–1481.
17. Reich NH, van Sark WGJHM, Turkenburg WC. Charge yield potential of indoor-operated solar cells incorporated into product integrated photovoltaic (PIPV). *Renewable Energy* 2011; **36**(2): 642–647.
18. Dirnberger D, Müller B, Reise C. PV module energy rating: opportunities and limitations. *Progress in Photovoltaics: Research and Applications* 2015; **23**(12): 1754–1770.
19. Heydenreich W, Müller B, Reise C. Describing the world with three parameters: a new approach to PV module power modelling, In *Proceedings of the 23rd European Photovoltaic Solar Energy Conference*, Valencia, Spain, 2008; 2786–2789.
20. John J, Rajasekar V, Boppana S, Tatapudi S, Tamizhmani G. Angle of incidence effects on soiled PV modules, In *Proc. SPIE 9179, Reliability of Photovoltaic Cells, Modules, Components, and Systems VII, 91790D*, 2014.
21. IEC 60904-3 (Ed 2.) Photovoltaic devices - Part 3: measurement principles for terrestrial photovoltaic (PV) solar devices with reference spectral irradiance data, 2008.
22. Schropp REI. *FW: IQE/EQE data HIT cellen*, 2014.
23. ten Kate OM, de Jong M, Hintzen HT, van der Kolk E. Efficiency enhancement calculations of state-of-the-art solar cells by luminescent layers with spectral shifting, quantum cutting, and quantum tripling function. *Journal of Applied Physics* 2013; **114**(8).
24. Alonso-Abella M, Chenlo F, Nofuentes G, Torres-Ramírez M. Analysis of spectral effects on the energy yield of different PV (photovoltaic) technologies: the case of four specific sites. *Energy* 2014; **67**: 435–443.
25. Nofuentes G, García-Domingo B, Muñoz JV, Chenlo F. Analysis of the dependence of the spectral factor of some PV technologies on the solar spectrum distribution. *Applied Energy* 2014; **113**: 302–309.
26. Sutterlueti J, Ransome S, Kravets R, Schreier L. Characterising PV modules under outdoor conditions: what's most important for energy yield, In *Proceedings of the 26th European Photovoltaic Solar Energy Conference and Exhibition*, WIP Renewable Energies, Aachen, Germany, Hamburg, Germany, 2011.
27. Huld T, Amillo AMG. Estimating PV module performance over large geographical regions: the role of irradiance, air temperature, wind speed and solar spectrum. *Energies* 2015; **8**(6): 5159–5181.
28. Hirata Y, Tani T. Output variation of photovoltaic modules with environmental factors-I. The effect of spectral solar radiation on photovoltaic module output. *Solar Energy* 1995; **55**(6): 463–468.
29. Ishii T, Otani K, Takashima T, Xue Y. Solar spectral influence on the performance of photovoltaic (PV) modules under fine weather and cloudy weather conditions. *Progress in Photovoltaics: Research and Applications* 2013; **21**(4): 481–489.
30. Nann S, Emery K. Spectral effects on PV-device rating. *Solar Energy Materials and Solar Cells* 1992; **27**(3): 189–216.
31. Cornaro C, Andreotti A. Influence of average photon energy index on solar irradiance characteristics and outdoor performance of photovoltaic modules. *Progress in Photovoltaics: Research and Applications* 2013; **21**(5): 996–1003.
32. Gottschalg R, Betts TR, Infield DG, Kearney MJ. On the importance of considering the incident spectrum when measuring the outdoor performance of amorphous silicon photovoltaic devices. *Measurement Science and Technology* 2004; **15**(2): 460.
33. Rüther R, Kleiss G, Reiche K. Spectral effects on amorphous silicon solar module fill factors. *Solar Energy Materials and Solar Cells* 2002; **71**(3): 375–385.
34. Ishii T, Otani K, Itagaki A, Utsunomiya K. A simplified methodology for estimating solar spectral influence on photovoltaic energy yield using average

DOI: 10.1002/pip

photon energy. *Energy Science & Engineering* 2013; **1**(1): 18–26.
35. Ishii T, Otani K, Itagaki A, Utsunomiya K. A methodology for estimating the effect of solar spectrum on photovoltaic module performance by using average photon energy and a water absorption band. *Japanese Journal of Applied Physics* 2012; **51**: 51(10NF05).
36. Kataoka N, Yoshida S, Ueno S, Minemoto T. Evaluation of solar spectral irradiance distribution using an index from a limited range of the solar spectrum. *Current Applied Physics* 2014; **14**(5): 731–737.
37. Chantana J, Ueno S, Ota Y, Nishioka K, Minemoto T. Uniqueness verification of direct solar spectral index for estimating outdoor performance of concentrator photovoltaic systems. *Renewable Energy* 2015; **75**: 762–766.
38. Minemoto T, Nakada Y, Takahashi H, Takakura H. Uniqueness verification of solar spectrum index of average photon energy for evaluating outdoor performance of photovoltaic modules. *Solar Energy* 2009; **83**(8): 1294–1299.
39. Moreno-Sáez R, Mora-López L. Modelling the distribution of solar spectral irradiance using data mining techniques. *Environmental Modelling & Software* 2014; **53**: 163–172.
40. Moreno Sáez R, Sidrach-de Cardona M, Mora-López L. Data mining and statistical techniques for characterizing the performance of thin-film photovoltaic modules. *Expert Systems with Applications* 2013; **40**(17): 7141–7150.
41. Twidell JW, Weir T. *Renewable Energy Resources*, 2nd edn. Taylor & Francis: London, 2010. reprinted.
42. King BH, Riley D, Robinson CD, Pratt L. Recent advancements in outdoor measurement techniques for angle of incidence effects, In *2015 IEEE 42nd Photovoltaic Specialist Conference (PVSC)*, New Orleans, LA, USA, 2015; 1–6.
43. Donovan M, Bourne B, Roche J. Efficiency VS. irradiance characterization of PV modules requires angle-of-incidence and spectral corrections, In *2010 35th IEEE Photovoltaic Specialists Conference (PVSC)*, Honolulu, HI, USA, 2010; 2301–2305.
44. Martin N, Ruiz JM. Calculation of the PV modules angular losses under field conditions by means of an analytical model. *Solar Energy Materials and Solar Cells* 2001-12; **70**(1): 25–38.
45. King DL, Kratochvil JA, Boyson WE. Measuring solar spectral and angle-of-incidence effects on photovoltaic modules and solar irradiance sensors, In *Conference Record of the Twenty-Sixth IEEE Photovoltaic Specialists Conference, 1997*, Anaheim, CA, USA, 1997; 1113–1116.
46. Balenzategui JL, Chenlo F. Measurement and analysis of angular response of bare and encapsulated silicon solar cells. *Solar Energy Materials and Solar Cells* 2005; **86**(1): 53–83.
47. Beal RJ, Potter BG, Simmons JH. Angle of incidence effects on external quantum efficiency in multicrystalline silicon photovoltaics. *IEEE Journal of Photovoltaics* 2014; **4**(6): 1459–1464.
48. Virtuani A, Lotter E, Powalla M. Performance of Cu(In,Ga)Se2 solar cells under low irradiance. *Thin Solid Films* 2003; **431-432**: 443–447.
49. Makrides G, Zinsser B, Georghiou GE, Schubert M, Werner JH. Temperature behaviour of different photovoltaic systems installed in Cyprus and Germany. *Solar Energy Materials and Solar Cells* 2009; **93**(6–7): 1095–1099.
50. Shah A, Meier J, Vallat-Sauvain E, Droz C, Kroll U, Wyrsch N, Guillet J, Graf U. Microcrystalline silicon and 'micromorph' tandem solar cells. *Thin Solid Films* 2002; **403-404**: 179–187.

  2017; **25**:218–232
DOI: 10.1002/pip